DRAFT SF 298

1. Report Date (dd-mm-yy)	2. Report Type	3. Dates covered (from... to)

4. Title & subtitle Chemistry, Structure and Morphology of Native and Passive Oxide Films on aluminum Rich Amorphous Al-Fe-Ce Alloys Tri-Service Conference on Corrosion Proceedings	5a. Contract or Grant #
	5b. Program Element #
6. Author(s) Mansour, A. N. Melendres C. A.	5c. Project #
	5d. Task #
	5e. Work Unit #

7. Performing Organization Name & Address	8. Performing Organization Report #
9. Sponsoring/Monitoring Agency Name & Address Tri-Service Committee on Corrosion USAF WRIGHT-PATTERSON Air Force Base, Ohio 45433	10. Monitor Acronym
	11. Monitor Report #

12. Distribution/Availability Statement
Approved for Public Release
Distribution Unlimited

13. Supplementary Notes

14. Abstract

15. Subject Terms
Tri-Service Conference on Corrosion

Security Classification of			19. Limitation of Abstract	20. # of Pages	21. Responsible Person (Name and Telephone #)
16. Report	17. Abstract	18. This Page			

TRI-SERVICE CONFERENCE ON CORROSION

21-23 JUNE 1994

SHERATON PLAZA HOTEL
ORLANDO, FLORIDA

PROCEEDINGS

Chemistry, Structure and Morphology of Native and Passive Oxide Films on Aluminum Rich Amorphous Al-Fe-Ce Alloys

Dr. A. N. Mansour*
Naval Surface Warfare Center, Code R34
10901 New Hampshire Avenue
Silver Spring, MD 20903-5000

Dr. C. A. Melendres
Argonne National Laboratory
Materials Science and Chemical Technology Divisions
Argonne, IL 60439-8111

Abstract

Aluminum based metallic glasses are of technological importance due to their high strength, low density, and anticipated high resistance to corrosion. We report on the corrosion characteristics such as corrosion potentials, corrosion currents, and pitting potentials of melt-spun ribbons of $Al_{90}Fe_{10-x}Ce_x$ ($x = 3,5,7$). In addition, we have examined the chemistry, structure, and morphology of the native and passive oxide films using X-ray Absorption Fine Structure Spectroscopy, X-ray Photoelectron Spectroscopy, and Scanning Electron Microscopy. Passive oxide films were induced by anodizing below the pitting potential in an aqueous solution of 0.9 wt% NaCl for 30 and 60 minutes using potentiodynamic polarization techniques.

Introduction

Aluminum based metallic glasses with remarkably high Al content are relatively new materials that were discovered independently by He et al.[1] and Tsai et al.[2] Typical composition is Al-TM-RE where TM is a late transition element such as iron, cobalt, or nickel and RE is a rare earth element such as yttrium, gadolinium or cerium. These amorphous alloys can be prepared with high aluminum content by rapid solidification

/

from the liquid phase using the melt-spinning method[1,2] or by vapor quenching using the dc magnetron sputtering method.[3] The amorphous phase is formed with an Al content as high as 90 atomic percent and are truly non-crystalline alloys which combine the properties of a metal with the short range order of a glass. They are very homogenous and lack the defects such as grain boundaries and dislocations typical of a crystalline material. The homogeneity and the lack of grain boundaries have led to a number of remarkable mechanical[4,5] and magnetic[6] properties. Amorphous ribbons of melt spun materials have high strength, ductility, and low density. It is also expected that, due to lack of grain boundaries, this material will have high resistance to corrosion. Consequently, these materials are potentially important metallic materials for many critical engineering applications.

In this paper, we report on the corrosion characteristics as well as the chemistry, structure and morphology of the native and passive oxide films of melt-spun $Al_{90}Fe_{10-x}Ce_x$ (x = 3, 5 and 7) using Scanning Electron Microscopy (SEM), X-ray Photoelectron Spectroscopy (XPS), and X-ray Absorption Fine Structure Spectroscopy (XAFS).

Experimental

Sample Preparation:

Amorphous samples in the form of 25 micron thick ribbons with nominal composition, $Al_{90}Fe_xCe_{10-x}$ (x = 3, 5 and 7), were prepared by rapid solidification from the liquid phase using the melt-spinning method. For comparison purposes, crystalline $Al_{90}Fe_3Ce_7$ was prepared from amorphous $Al_{90}Fe_3Ce_7$ by heating in an inert atmosphere.

Corrosion Measurements:

Corrosion characteristics such as corrosion potentials, corrosion currents and pitting potentials of these alloys were determined by means of potentiodynamic polarization measurements made on samples immersed in an aqueous solution of 0.9 wt% NaCl (0.15M). The measurements on the alloys were compared with those of pure aluminum and iron. Passive films were formed in the 0.9 wt% NaCl solution by anodizing below the pitting potential for 30 and 60 minutes. Passivation of $Al_{90}Fe_7Ce_3$ was also induced in 3.5 Wt% (0.6 M) NaCl by anodizing below the pitting potential for 30 minutes. The passivated samples were

then pulled from the solution and dried in a stream of nitrogen gas. The effect of sample rinsing with copious amounts of deionized H_2O on the chemistry and structure of passive films was also investigated.

SEM Measurements:

An Amray 1000A scanning electron microscope (SEM) was used to investigate the morphology of control (no passivation) and passivated alloys. An electron beam at a voltage of 20 KeV, current of 0.01 na, and a diameter of the order of 100 Å was employed. Compositional analyses were made by means of Energy Dispersive Analysis of X-Rays (EDAX). At the conditions of our experiment, the EDAX determined composition represents that of the bulk (roughly 2μm deep). Experiments were performed at a system pressure less than 10^{-6} Torr.

XPS Measurements:

XPS spectra were collected using a Perkin-Elmer/Physical Electronics Division photoelectron spectrometer (model 5400) under computer control. All spectra were obtained with monochromatized Al x-rays ($h\nu = 1486.6$ eV). The anode operated at 15 KV drawing a current of 40 mA. The composition and chemistry of the native oxide films were investigated using angle resolved XPS. During the XPS measurements, the analysis chamber pressure was kept in the range of $(1\text{-}3)\times10^{-8}$ Torr. The XPS data were collected from an analysis area of 1mm x 1mm. All binding energies were referenced to the C 1s photoelectron line for adventitious hydrocarbon set at 285.0 eV.

XAFS Measurements:

The X-ray absorption experiments were performed on beamline X-11A of the National Synchrotron Light Source (NSLS) at Brookhaven National Laboratory (BNL) with the electron storage ring operating at an electron energy of 2.5 GeV and a stored current in the range of 110 to 220 mA.[7] Data were collected with a variable exit double-crystal monochromator using two flat Si(111) crystals. Spectra of the Ce L_3-edge and Fe K-edge data for the alloys were obtained using transmission, fluorescence[8] and total electron yield[9] detection modes. The fluorescence and total electron yield data were obtained using a specialized fluorescence ion chamber detector[10] and total electron yield detector,[11] respectively. The X-ray intensities were monitored using

ionization chambers filled with nitrogen gas for the incident beam, an appropriate mixture of nitrogen and argon gases for the transmitted beam and krypton gas for fluorescence signal. The electron yield detector had helium gas. The background component due to elastic and Compton scattering of the incident X-rays was minimized by using an aluminum Soller slit assembly and V and Mn filters, each with an effective thickness of three absorption lengths, for the Ce L_3-edge and Fe K-edge, respectively. Due to surface sensitivity of the electron yield data and, hence, enhanced sensitivity to the passive film structure, only the electron yield spectra for the passivated alloys will be discussed in this paper. The energy calibration for Fe, and Ce was monitored using a Fe foil and a CeO_2 reference and employing a third ion chamber filled with the same gas as that of the transmitted beam ion chamber.

Reference samples of bulk Fe (5 μm thick foil), Fe_2O_3, $Ce(NO_3)_3$, and CeO_2 were also investigated to serve as standards for comparison and subsequent data analysis. The XAFS measurements for the Fe foil, Fe_2O_3, $Ce(NO_3)_3$, and CeO_2 were made in the transmission mode. Research grade Fe_2O_3, $Ce(NO_3)_3$, and CeO_2 were prepared for the x-ray absorption measurements by grinding into a fine powder and selecting particles less than 20μm by sieving through a 20 μm size nylon screen. The fine powder was then deposited on Kapton tape and several layers were then stacked to give a relatively uniform thickness appropriate for XAFS measurements. Two and four layers were used in separate runs for Fe_2O_3 giving a $\Delta\mu x$ of 0.53 and 1.00, respectively. Six layers were used for $Ce(NO_3)_3$ giving a $\Delta\mu x$ of 0.64. Six layers were used for CeO_2 giving a $\Delta\mu x$ of 0.81. All spectra were measured at room temperature (300 K).

Results

Potentiodynamic Polarization Studies:

Figure 1 shows typical anodic dissolution/passivation curves for amorphous and recrystallized $Al_{90}Fe_3Ce_7$. A summary of corrosion potentials, corrosion currents and pitting potentials for the alloys as a function of composition and for pure crystalline aluminum and iron foils is presented in Table I. The corrosion potentials are nearly the same for the alloys and pure aluminum while the corrosion currents (hence, corrosion rates) for the amorphous alloys are larger than that for pure aluminum. The corrosion current for amorphous $Al_{90}Fe_3Ce_7$ is significantly

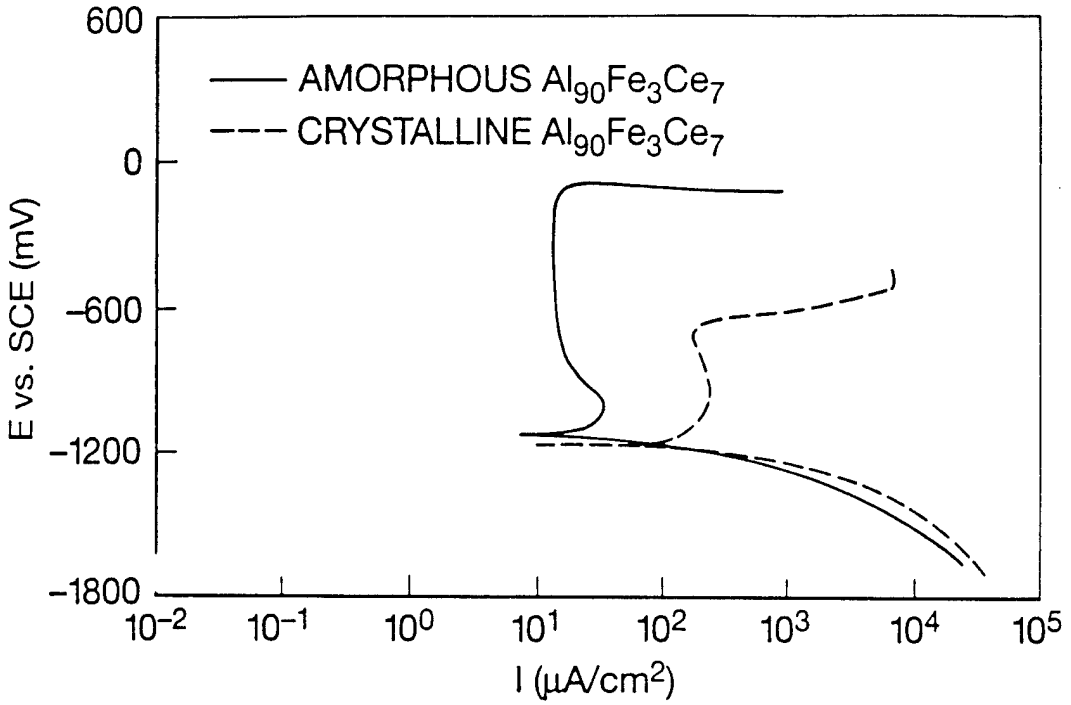

Figure 1. Typical anodic dissolution/passivation curves for amorphous and recrystallized $Al_{90}Fe_3Ce_7$.

Table I. Corrosion potentials, corrosion currents and pitting potentials for liquid-quenched alloys immersed in an aqueous solution of 0.9 wt% NaCl.

Composition	Structure	$E_{corrosion}$ (mV vs. SCE*)	$I_{corrosion}$ (μV/cm^2)	$E_{pitting}$ (mV vs. SCE*)
$Al_{90}Fe_7Ce_3$	Amorphous	-1075	325	-150
$Al_{90}Fe_5Ce_5$	Amorphous	-1028	65	-100
$Al_{90}Fe_3Ce_7$	Amorphous	-1079	20	-90
	Crystallized	-1167	851	-675
Al metal	Crystalline	-1046	0.15	-700
Fe metal	Crystalline	-500	42	-225

* SCE ≡ Saturated Calomel Electrode.

smaller than that of crystalline $Al_{90}Fe_3Ce_7$ which is probably due to lack of grain boundaries in the amorphous state as will be shown later from SEM micrographs. The corrosion currents for the amorphous alloys also decrease with increase in cerium content. Pitting potentials for the amorphous alloys are more positive than that for pure aluminum or crystalline $Al_{90}Fe_3Ce_7$ alloy indicating that the physical and chemical nature of passive films for the amorphous alloys are more resistant to pitting than for pure aluminum and crystallized alloys.

SEM Studies:

Figure 2 shows a comparison of SEM micrographs for amorphous and recrystallized $Al_{90}Fe_3Ce_7$ indicating the lack of grain boundaries in the amorphous state in contrast to the crystalline state. Figure 3 shows SEM micrographs for the control (no passivation) and passivated amorphous $Al_{90}Fe_7Ce_3$. Again, these micrographs display no grain boundaries revealing the amorphous nature of the alloys. EDAX elemental analysis confirms that the few crystallites displayed by the SEM micrograph on the surface of passivated $Al_{90}Fe_7Ce_3$ (Figure 3) represent contamination by NaCl crystallites from the solution.

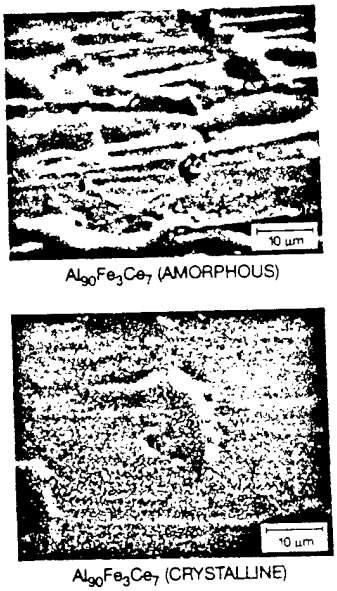

$Al_{90}Fe_3Ce_7$ (AMORPHOUS)

$Al_{90}Fe_3Ce_7$ (CRYSTALLINE)

Figure 2 SEM micrographs for amorphous and recrystallized $Al_{90}Fe_3Ce_7$.

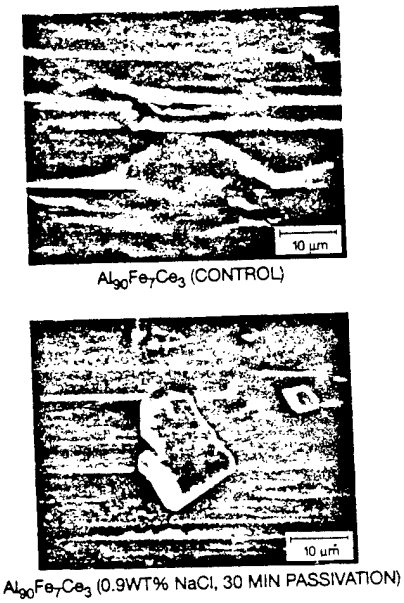

$Al_{90}Fe_7Ce_3$ (CONTROL)

$Al_{90}Fe_7Ce_3$ (0.9WT% NaCl, 30 MIN PASSIVATION)

Figure 3 SEM micrographs for the control and passivated amorphous $Al_{90}Fe_7Ce_3$.

A summary of elemental concentrations, in atomic percent, as determined by EDAX is listed in Table II.

Table II. Elemental concentrations for amorphous (A) and recrystallized (C) alloys in the as received conditions (control) and after passivation by anodizing below the pitting potential: a) in 0.9 wt% NaCl for 30 minutes (PS #1) and 60 minutes (PS #2) and b) in 3.5 wt% NaCl for 30 minutes (PS #3). Concentrations in parentheses correspond to Al, Fe and Ce normalized to 100% to allow for comparison with those for the control samples.

Sample	Treat.	Concentration (atomic percent)					
		Al	Fe	Ce	Cu	Na	Cl
$Al_{90}Fe_7Ce_3$ (A)	Control	88.5	7.4	3.7	0.4		
	PS #1	80.8 (86.4)	8.2 (8.8)	4.5 (4.8)	0.6	3.7	2.3
	PS #2	74.7 (84.0)	9.1 (10.2)	5.1 (5.7)	0.5	9.6	1.0
	PS #3	77.2 (86.8)	7.6 (8.5)	4.1 (4.6)	0.4	8.4	2.3
$Al_{90}Fe_5Ce_5$ (A)	Control	88.3	5.1	6.1	0.5		
	PS #1	80.7 (84.9)	6.6 (6.9)	7.7 (8.1)	0.5	4.1	0.4
	PS #2	79.7 (86.6)	6.0 (6.5)	6.3 (6.8)	0.6	6.5	0.9
$Al_{90}Fe_3Ce_7$ (A)	Control	88.8	3.2	7.9	0.1		
	PS #1	82.3 (85.8)	3.9 (4.1)	9.7 (10.1)	0.0	3.3	0.8
	PS #2	76.7 (85.9)	3.6 (4.0)	9.0 (10.1)	0.2	6.8	3.7
$Al_{90}Fe_3Ce_7$ (C)	Control	88.9	3.0	7.9	0.1		

The copper impurity is an artifact of the sample preparation procedure which employs a copper wheel as part of the melt spinning apparatus; sodium and chlorine are observed in the analysis of passivated samples and are due to contamination from the aqueous NaCl solution. The concentrations for the control samples are in good agreement with nominal compositions aimed for during sample preparation. A slight decrease in the Al content and a significant increase in the Fe and Ce concentrations for the passivated alloys relative to the control alloys are observed suggesting segregation of both Fe and Ce from the bulk into the near surface region as a result of the passivation procedure.

XPS Studies:

Survey spectrum, high resolution multiplexes of the C 1s, O 1s, Al 2p, Al 2s, Fe 2p, and Ce 3d photoelectron lines and the valence band region, and Al 2p, Al 2s and O 1s angle resolved XPS spectra for the control $Al_{90}Fe_7Ce_3$ have been published elsewhere[12]; these will only be briefly discussed here. Figures 4 and 5 show angle resolved XPS spectra of Al 2p and O 1s photoelectron lines for control $Al_{90}Fe_7Ce_3$. Angle resolved spectra of the Al 2p and O 1s photoelectron lines were measured for θ (electron emission angle as measured relative to sample plane) = 80, 78, 75, 70, 65, 60, 55, 45, 35, 25, 15, 5. The Al 2p spectra display two components with strong dependence on electron emission angle. It is shown that the intensity of the high binding energy component increases with decrease in θ in contrast with the low binding energy component whose intensity decreases with decrease in θ. Thus, the high binding energy component at $\approx$ 74.5 eV corresponds to oxidized Al in the native oxide film. The low binding energy component at $\approx$ 71.6 , on the other hand, corresponds to Al in $Al_{90}Fe_7Ce_3$ underlying the native oxide film. Angle resolved spectra of the O 1s photoelectron line consists of an asymmetric peak due to the presence of two sub-peaks which are not quite resolved from each other but were resolved using standard curve fit analysis procedures. Based on curve fit analysis, two components with binding energies of $\approx$ 531.2 and 532.4 eV were resolved corresponding to hydroxyl groups and ionic oxygen indicating that the composition and chemistry of the native oxide can be depicted as $AlO_x(OH)_y$. The O 1s spectra show that the intensity ratio of the peak corresponding to hydroxyl groups to that of ionic oxygen decreases with increase in θ The observed angle dependencies for both the Al and O 1s lines are consistent with a layered structure in which the $Al_{90}Fe_7Ce_3$ alloy

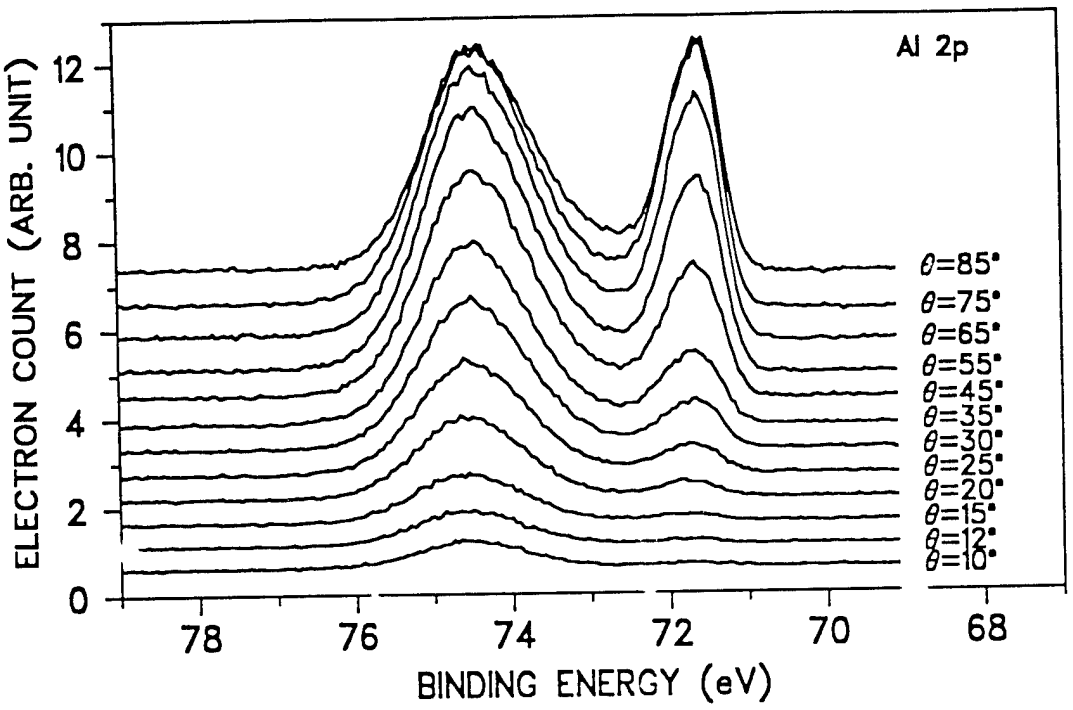

Figure 4. Angle resolved XPS spectra of Al 2p for control $Al_{90}Fe_7Ce_3$.

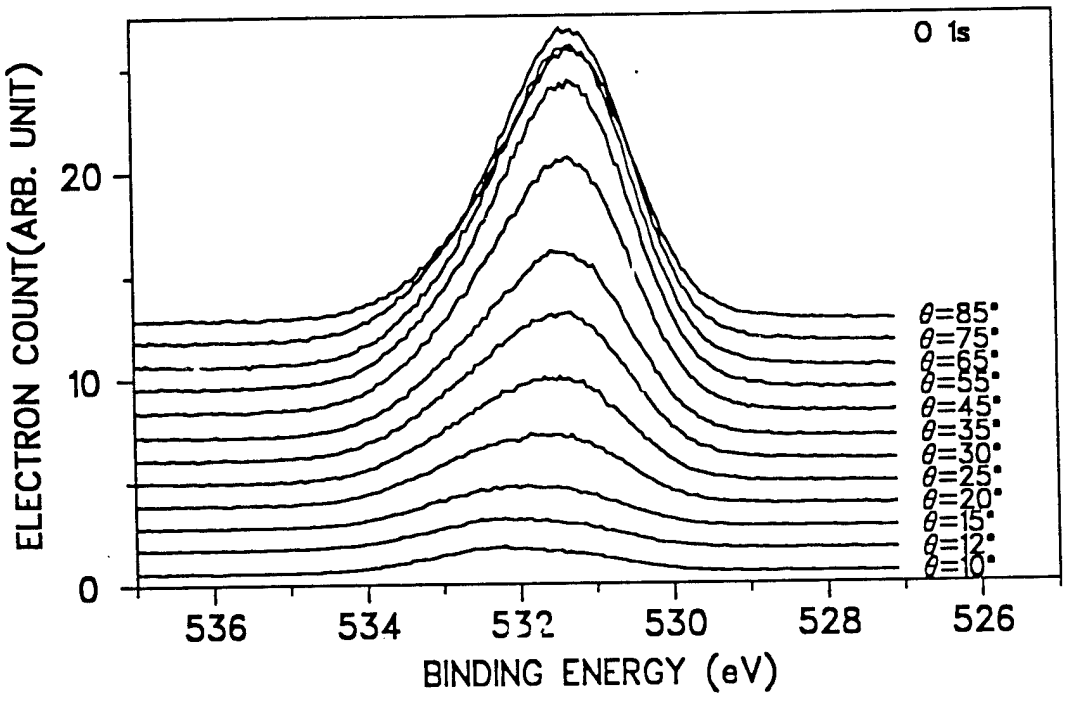

Figure 5. Angle resolved XPS spectra of O 1s for control $Al_{90}Fe_7Ce_3$.

is covered with native oxide of $AlO_x(OH)_y$. The angle resolved XPS data can also be used to determine the film thickness of the native oxide.

XPS spectra of passivated alloys in 0.9 wt% NaCl solution for 60 minutes and then dried in a stream of dry nitrogen gas show that the Fe and Ce concentrations in the near surface region have significantly increased relative to their concentrations in the control alloys.[13] Figures 6, 7, and 8 show comparisons spectra of Al 2p, Fe 2p and Ce 3d XPS spectra, respectively, taken at electron emission angle, θ = 45°, for control $Al_{90}Fe_7Ce_3$ and passivated $Al_{90}Fe_7Ce_3$ as well as passivated $Al_{90}Fe_3Ce_7$ in aqueous 0.9 wt% NaCl for 60 minutes. The Al 2p spectra for passivated alloys display a broad peak corresponding to oxidized Al in contrast to the control spectrum which display two components corresponding to oxidized and metallic Al. The Fe 2p spectrum of control $Al_{90}Fe_7Ce_3$ displays the spin orbit doublet ($2p_{1/2}$ and $2p_{3/2}$) with binding energies characteristic of metallic Fe. The Fe 2p spectra for passivated $Al_{90}Fe_7Ce_3$ and $Al_{90}Fe_3Ce_7$ show broad peaks which are shifted to higher binding energies relative to those of the control spectra. Based on comparison of the Fe 2p binding energies and their characteristic shake-up with reference spectra for Fe in various phases,[14,15,16,17,18] we conclude that the Fe chemistry in the passive film

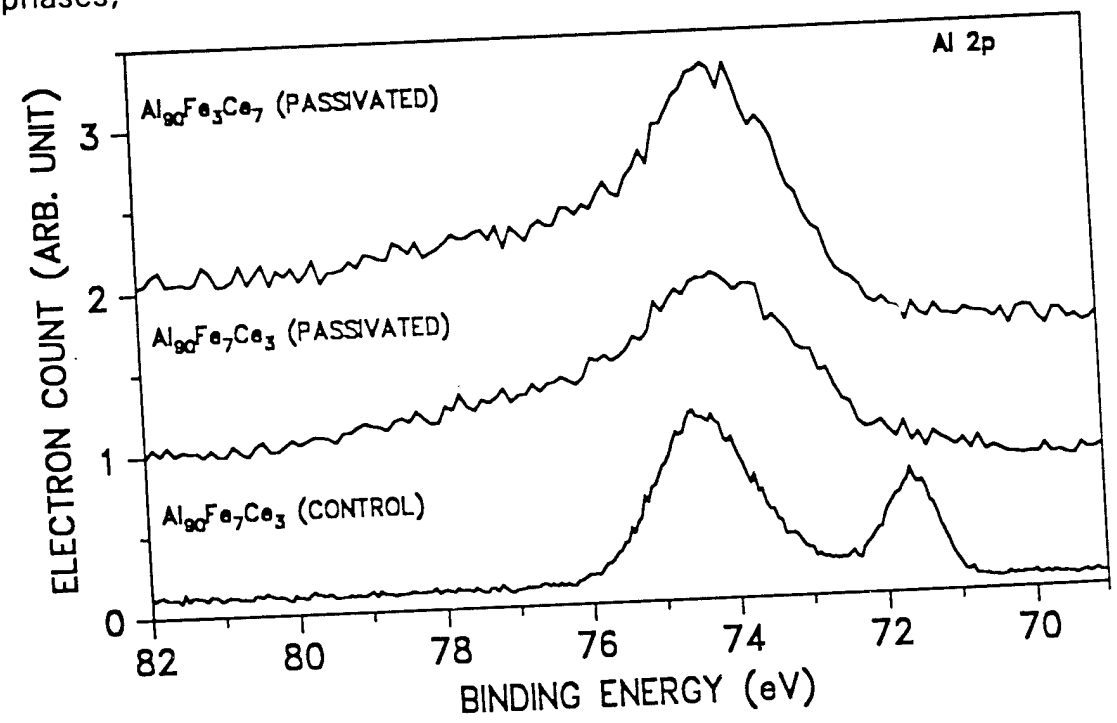

Figure 6. XPS spectra of Al 2p for control and passivated alloys.

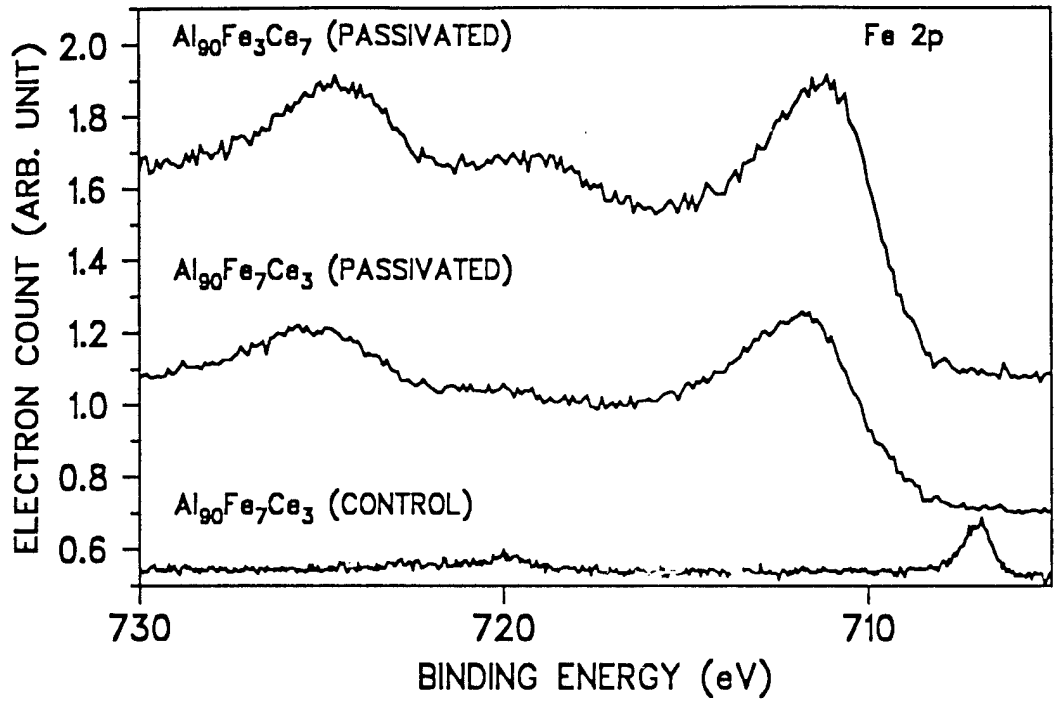

Figure 7. XPS spectra of Fe 2p for control and passivated alloys.

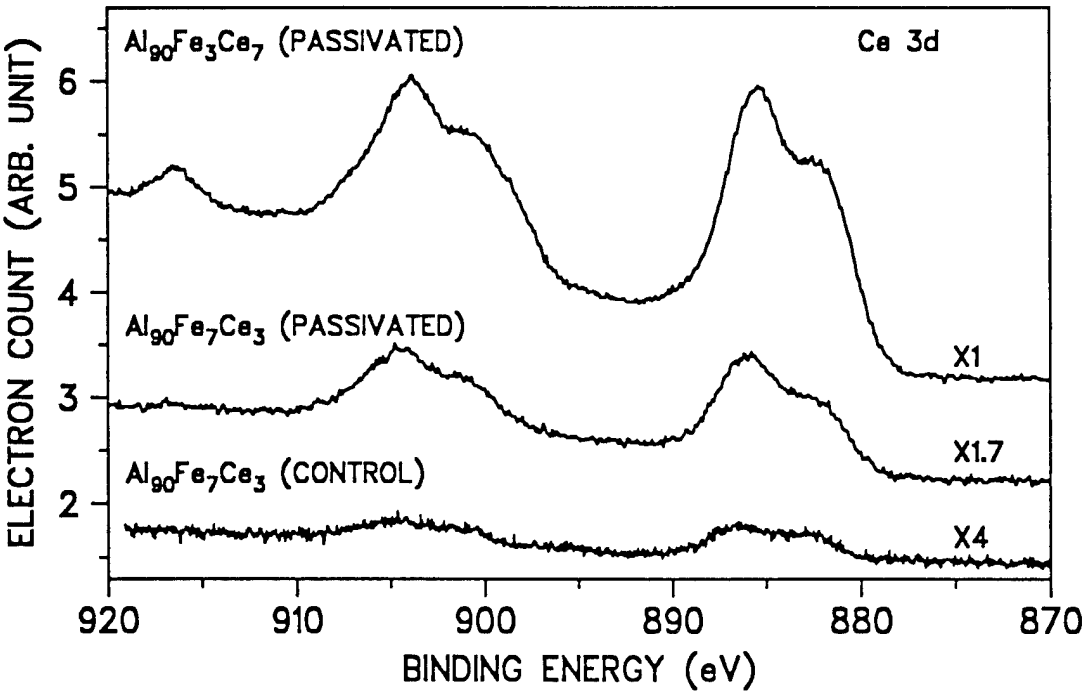

Figure 8. XPS spectra of Ce 3d for control and passivated alloys.

is similar to that of Fe in Fe_3O_4 for $Al_{90}Fe_7Ce_3$ and Fe in α-Fe_2O_3 or FeOOH for $Al_{90}Fe_3Ce_7$.

The Ce 3d spectra of Figure 8 display broad lines for each of the $3d_{3/2}$ (high binding energy component) and $3d_{5/2}$ (low binding energy component) spin orbit doublet. The shoulders on the low binding energy side for each component corresponds to the well known shake-down structure.[19,20,21,22,23] Based on the binding energy of the principal lines, the nature of the shake down structure, and the magnitude of the spin orbit splitting we conclude that the oxidation state of Ce in the passive film for $Al_{90}Fe_7Ce_3$ and $Al_{90}Fe_3Ce_7$ is mainly +3, i.e., similar to that of Ce in Ce_2O_3 or $Ce(OH)_3$. A peak at roughly 916 eV in the Ce 3d spectrum for $Al_{90}Fe_3Ce_7$ is characteristic of Ce in the +4 oxidation state such as that of Ce in CeO_2. Hence the chemistry of a fraction of Ce in the passive film of $Al_{90}Fe_3Ce_7$ is similar to that of Ce in CeO_2.

XAFS Studies:

Figures 9 and 10 show the Fe K-edge and Ce L_3-edge XANES spectra, respectively, for control alloys and alloys passivated in 0.9 wt% NaCl for 60 minutes and then dried in a stream of dry nitrogen gas. The Fe K-edge spectra were compared with the reference spectrum of structurally well defined α-Fe_2O_3. The Fe K-edge spectra for the passivated alloys are clearly distinct from those of control alloys but resemble more closely the spectrum of α-Fe_2O_3. Note that the XANES spectra of Fe_3O_4, α-Fe_2O_3, γ-Fe_2O_3, and γ-FeOOH are very similar and can not be distinguished from each other. In all of these compounds the oxidation state of Fe +3 except for Fe_3O_4 where one-third of Fe is present in the +2 and two-thirds of Fe is present in the +3 oxidation states. Hence, the oxidation state of the majority of Fe in the passive film is +3. The Ce L_3-edge spectra of Figure 10 were compared with reference spectra of structurally well defined $Ce(NO_3)_3$ and CeO_2. It is shown that the spectra of passivated alloys are clearly distinct from those of the control alloys. The Ce L_3-edge spectrum for passivated $Al_{90}Fe_7Ce_3$ resemble more closely that of $Ce(NO_3)_3$ while that of passivated $Al_{90}Fe_3Ce_7$ is identical to that of CeO_2. The spectrum for passivated $Al_{90}Fe_5Ce_5$ is intermediate between those of $Ce(NO_3)_3$ and CeO_2. Based on these results we conclude that the oxidation state of Ce in the passive film of $Al_{90}Fe_7Ce_3$ is mainly +3 with only a small amount of Ce in +4 state. The majority of Ce is present in the +3 oxidation state with the remainder being present in the +4 oxidation state in the

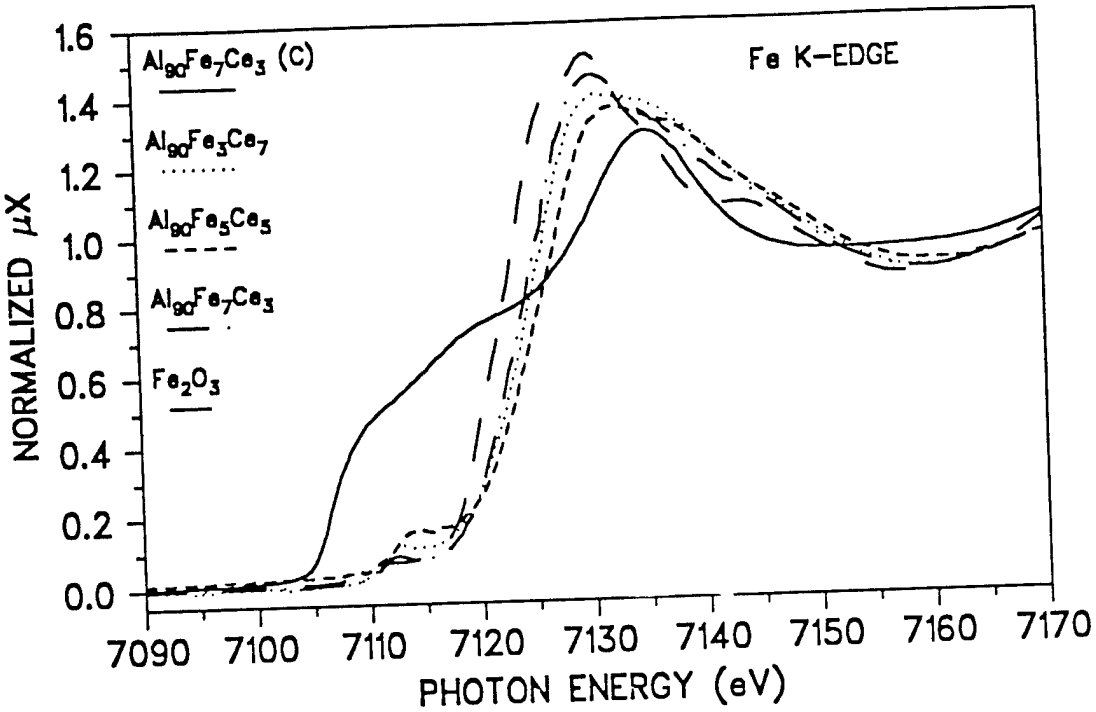

Figure 9. XANES spectra of Fe K-edge for control (C) and passivated alloys and α-Fe_2O_3

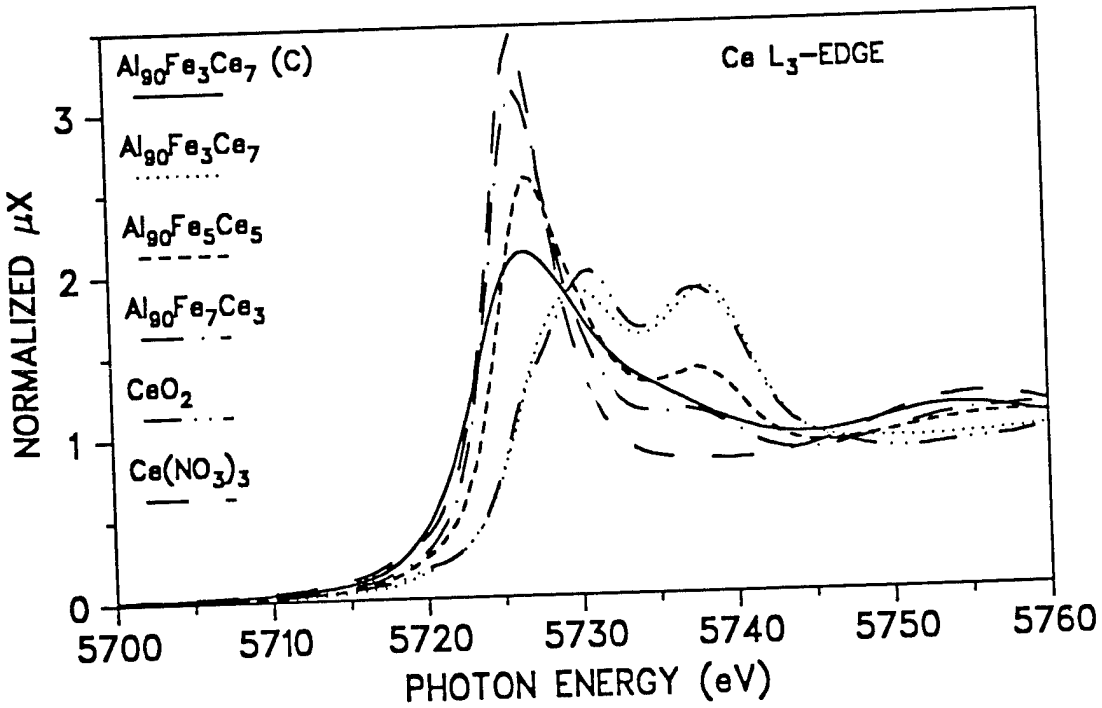

Figure 10. XANES spectra of Ce L_3-edge for control (C) and passivated alloys, $Ce(NO_3)_3$ and CeO_2.

passive film for $Al_{90}Fe_5Ce_5$. For $Al_{90}Fe_3Ce_7$, Ce in the passive film is present only in the +4 oxidation state. This indicates that the fraction of Ce in the +4 oxidation state increases with increase in the Ce content of the alloy. XANES spectra of passivated alloys rinsed with copious amounts of deionized H_2O (not shown here) show that the fraction of Ce in the +3 oxidation state decreased relative to those for samples dried in a stream of nitrogen gas. Thus, the effect of H_2O rinsing on the chemistry of Ce in the passive film region is to oxidize a fraction of Ce present in the +3 state to Ce in the +4 state. No change in the chemistry of Fe is observed in samples rinsed with copious amounts of deionized H_2O vis. samples dried in a stream of dry nitrogen gas.

Acknowledgement

This work was supported by the Independent Research Program of NSWCDD (ANM), and the U. S. Department of Energy, Materials Science Division, (CAM). We acknowledge the support of the U.S. Department of Energy, Division of Materials Sciences, under Contract Number DE-AS05-80-ER-10742 for its role in the development and operation of beam line X-11A at the National Synchrotron Light Source (NSLS). The NSLS is supported by the Department of Energy, Division of Materials Sciences and Division of Chemical Sciences, under Contract Number DE-AC02-76CH00016. We are also greatful to Professor S. J. Poon, Dr. Y. He, and Professor G. J. Shiflet of the University of Virginia, Charlottesville, VA 22903-2458 for providing the samples used in this investigatior The work at UV was supported by the U. S. Army Research Office under contract no. DAAH-94-G-0076. In addition, we are thankful to Dr. R. A. Brizzolara of NSWC for assistance during the XAFS data acquisition at BNL and to Dr. M. K. Norr also of NSWC for taking the SEM micrographs and EDAX analysis.

References

1. Y. He, S. J. Poon, and G. J. Shiflet, Science **241**, 1640 (1988).

2. A.-P. Tsai, A. Inoue, and T. Masumoto, Metallurgical Transactions A **19A**, 1369 (1988).

3. L. T. Kabacoff, C.-P. Wong, N. L. Guthrie, and S. Dallek, Mat. Sc. Eng. **A134**, 1288 (1991).

4. G. J. Shiflet, Y. He., and S. J. Poon, J. Appl. Phys. **64(12)**, 6863 (1988).

5. A. Inoue, K. Ohtera, and A.-P. Tsai, Jap. J. Appl. Phys. **27(4)**, 938, L479 (1988).

6. J. L. Wagner, K. M. Wong, F. S. Pierce, and S. J. Poon, Phys. Rev. B **39(8)**, 5500 (1989).

7. D.E. Sayers, S.M. Heald, M.A. Pick, J.I. Budnick, E.A. Stern, and J. Wong, Nucl. Instr. and Meth., **208**, 631 (1983).

8. J. Jaklevic, J.A. Kirby, M.P. Klein, A.S. Robertson, G.S. Brown, and P. Eisenberger, Solid State Communications, **23**, 679 (1977).

9. M. E. Kordesh and R. W. Hoffman, Phys. Rev. **B31**, 191 (1984).

10. F.W. Lytle, R.B. Greegor, D.R. Sandstrom, E.C. Marques, J. Wong, C.L. Spiro, G.P. Huffman, and F.E. Huggins, Nucl. Instr. and Meth., **226**, 542 (1984).

11. F. W. Lytle, R. B. Greegor, G. H. Via, J. M. Brown, and G. Meitzner, J. De Physique, Colloque C8, **47**, C8-149 (1986).

12. A. N. Mansour, S. J. Poon, and Y. He, and G. J. Shiflet, Surface Science Spectra **2**, 31 (1993).

13. A. N. Mansour, C. A. Melendres, M. Pankuch, S. J. Poon, Y. He, and G. J. Shiflet, Surface Science Spectra, **2**, in press, (1994).

14. H. Konno and M. Nagayama, Passivity of Metals: Proceedings of the 4th International Symposium on Passivity, (Princeton, NJ: Electrochemical Society, 1978), editors: R. B. Frankental and J. Kruger, p. 585.

15. V. Stambouli, C. Palacio, H. J. Mathieu, and D. Landolt, Appl. Surf. Sce. **70/71**, 240 (1993).

16. K. Assami and K. Hashimoto, Corrosion Science **17**, 559 (1077).

17. G. C. Allen, M. T. Curtis, A. J. Hooper, and P. M. Tucher, J. C. S. Dalton, 1525 (1974).

18. T. L. Barr, J. Phys. Chem. **82**, 1801 (1978).

19. P. Burroughs, A. Hamnett, A. F. Orchard,, and G. Thornton, J. Chem. Soc. Dalton **17**, 1686 (1976).

20. T. L. Barr and C. G. Fries, J. Chem. Soc. Dalton Trans., 1825 (1983).

21. L. Schlapbach and J. Osterwalder, Solid State Communications **42**, 271 (1982).

22. D. L. Perry and L. Tsao, J. Mat Sci Lett. **3**, 1017 (1984).

23. D. D. Sarma and C. N. Rao, J. Electron Spectrosc. and Related Phenomena **20**, 25 (1980).